e-J. Surf. Sci. Nanotech. Vol. 13 (2015) 129-134 Conference - ISSS-7 -

DFT Study of CO Oxidation Catalyzed by Au/TiO_2: Activity of Small Clusters*

Hiroaki Koga†
Elements Strategy Initiative for Catalysts and Batteries (ESICB), Kyoto University, 1-30 Goryo-Ohara, Kyoto 615-8245, Japan

Kohei Tada
Department of Chemistry, Graduate School of Science, Osaka University, 1-1 Machikaneyama, Toyonaka, Osaka 560-0043, Japan

Mitsutaka Okumura
Department of Chemistry, Graduate School of Science, Osaka University, 1-1 Machikaneyama, Toyonaka, Osaka 560-0043, Japan, and Elements Strategy Initiative for Catalysts and Batteries (ESICB), Kyoto University, 1-30 Goryo-Ohara, Kyoto 615-8245, Japan

(Received 7 January 2015; Accepted 23 February 2015; Published 28 March 2015)

CO oxidation over a rutile TiO_2(110) surface supporting a tetrahedral Au_{10} cluster has been examined by plane-wave DFT calculations. O_2 adsorbs sideon to the pentacoordinate Ti site of the oxide support with a large energy gain ($\sim$ 2 eV), activated to a peroxide state. O_2 adsorption on the cluster is much weaker. The stability and activation state of sideon O_2 depends weakly on distance to the cluster. On a Ti site next to the cluster, a sideon O_2 reacts with CO adsorbed on the cluster to yield CO_2 with a very small energy barrier of 0.13 eV. On a more remote Ti site, a sideon O_2 reacts with a gaseous CO to yield CO_2 with a barrier of 0.55 eV. Thus, O_2 + CO reaction is much faster at the perimeter even for a small cluster such as Au_{10}. Similar results are obtained for a truncated pyramidal Au_9, except that a carbonate is formed at the perimeter. The carbonate formation is inhibited if H_2O is adsorbed next to O_2. [DOI: 10.1380/ejssnt.2015.129]

Keywords: Density functional theory; Catalysis; Gold; Titanium oxide; Oxidation; Carbon monoxide; Oxygen; Clusters

I. INTRODUCTION

Gold nanoparticles ($\sim$ 3 nm in diameter) supported on metal oxides such as TiO_2 exhibit excellent catalytic activities toward low-T CO oxidation [1,2] and other important reactions [3]. Because gold generally lacks the ability to adsorb and activate O_2, it is viewed that reactions occur at the perimeter of a Au nanoparticle where it adjoins the oxide surface [4]. For a well-studied example of Au/TiO_2 at least, this has been supported by experiments showing the proportionality between the rate of CO oxidation and the length of the perimeter [5,6]. Yet, it is unclear whether this picture applies to supported clusters of smaller sizes ($\sim$ 1 nm in diameter). This question is becoming more important with growing interest in the size- and shape-specific activity of small Au clusters [3].

In the field of heterogeneous catalysis, computational methods such as density-functional theory (DFT) [7,8] are indispensable for identifying reaction sites, active species, and reaction paths. There are now a number of DFT studies (and joint ones) on CO oxidation over Au/rutile TiO_2 [9-16]. Earlier DFT calculations for supported Au nanorods [9,10] have shown that O_2 adsorbs and activates on the pentacoordinate Ti site (Ti^{5c}) of the oxide surface. This is because the strong positive field of the Ti cation lowers O_2 π^* states and induces electron transfer from the Au to O_2, resulting in Ti–O_2 ionic bonding and O–O bond weakening; naturally, the TiO_2 surface itself is unable to adsorb O_2 in the absence of electron donors such as Au clusters and O vacancies. It is considered that O_2 adsorbs preferentially at the perimeter because of Au-O_2 ionic interactions [9,14], but adsorption on more remote sites ('off-perimeter') is possible. Indeed, a DFT study for TiO_2-supported Au_N clusters ($N \leq 7$) [17] noted that O_2 adsorbs on a Ti^{5c} site that is not directly next to a cluster. However, reactions by such O_2 have been neglected in most DFT studies.

In our previous work [18], we have examined CO oxidation over a TiO_2-supported Au nanorod by DFT and found that an off-perimeter O_2 reacts with CO(g) with an energy barrier of 0.57 eV; (g) denotes a gaseous molecule. The perimeter hypothesis still holds because an on-perimeter O_2 reacts with a Au-adsorbed CO (Au-CO) with a smaller barrier of 0.22 eV. The aim of the present DFT study is to examine how the balance between these on- and off-perimeter reactions changes when the supported Au particle is downsized to $\sim$ 1 nm. Since it is impractical to study all the possible sizes and shapes of Au clusters, we use a tetrahedral Au_{10} as a model of small FCC clusters. This is a minimal FCC cluster and a building block for magic clusters such as 20-atom tetrahedron and 55-atom icosahedron. For comparison, we also briefly examine a truncated pyramidal Au_9 cluster.

The rest of this paper is organized as follows. Section II describes the details of calculation. Section III.A examines O_2 adsorption on Au_{10}/TiO_2 and finds that off-perimeter O_2 are nearly as stable as on-perimeter O_2. Section III.B examines CO oxidation on Au_{10}/TiO_2 and finds that an on-perimeter O_2 reacts with Au-CO with a very small barrier while an off-perimeter O_2 reacts with CO(g) with a barrier similar to that obtained for the supported rod. Section IV examines CO oxidation on Au_9/TiO_2 and finds that a carbonate is formed at the perimeter. Sec-

* This paper was presented at the 7th International Symposium on Surface Science, Shimane Prefectural Convention Center (Kunibiki Messe), Matsue, Japan, November 2-6, 2014.

† Corresponding author: koga.hiroaki.6u@kyoto-u.ac.jp, +81-75-383-3043 (phone), +81-75-383-3047 (fax)

tion V summarizes and concludes that O_2 + CO reaction is much faster at the perimeter also for small clusters such as Au_9 and Au_{10}.

II. DETAILS OF CALCULATION

As in our previous work [18], total energies and optimized geometries were calculated by STATE [19], a plane-wave DFT code. This code has been applied to a wide range of systems including Au/TiO_2 [20,21]. Ultrasoft pseudopotentials [22] and the exchange-correlation functional by Perdew, Burke, and Ernzerhof [23] were used. Kohn-Sham orbitals and the charge density were expanded into plane waves up to the cutoff energies of 25 and 225 Ry, respectively. The number of valence electrons was 1, 4, 6, 10, and 11 for H, C, O, Ti, and Au, respectively. Unless otherwise noted, the spin unpolarized (polarized) state was calculated for a system with an even (odd) number of electrons. The transition state (TS) of a reaction was searched by constrained optimization and then refined by force inversion [24]. The initial and final states (IS and FS) of the reaction were found by relaxation from TS. If this resulted in the detachment of a molecule from the surface, then the desorption limit was identified as IS/TS, and its total energy was obtained as the sum of total energies of the gaseous molecule and the rest, calculated separately. The Bader method [25,26] was used to determine the charge (and spin charge) carried by each atom. Negative charge on O_2 and the O-O bond length were used as indicators of O_2 activation state. Note that the Bader charge may differ from the formal oxidation number, e.g., the Bader charge on O of TiO_2 is calculated to be -1.1e. The charge density was visualized using VESTA [27]. The total energy of a gaseous molecule was calculated using a 24-Bohr cubic cell; O_2 was calculated as a triplet.

Figure 1(a) shows the Au_{10}/TiO_2 model used in the present study. The rutile TiO_2(110) surface was represented as a four-trilayer slab placed in a 2×4 cell (sampled at 1×2 k-point mesh). The thickness of a vacuum layer was 1.39 nm. The atoms of the bottom trilayer were constrained to their bulk positions. A tetrahedral Au_{10} cluster was placed on this surface with the orientation of Au(111)[110] ∥ TiO_2(110)[001]. This choice reduces the lattice mismatch along the Au-Au bond to less than 2%. The average distance between the bottom facet of Au_{10} and the uppermost Ti layer is calculated to be 0.31 nm, similar to 0.33 nm measured for Au nanoparticles deposited on TiO_2 [28]. Naturally, it is difficult to prove that this is the most stable geometry for the supported Au_{10}, but at least this is 0.24 eV more stable than a planar geometry shown in Fig. 1(b). The Au_9/TiO_2 model was obtained from Au_{10}/TiO_2 by removing the Au atom at the apex (Fig. 1(c)).

The adsorption energy is referenced to the desorption limit of O_2, CO, and/or H_2O. In our convention, a more stable state has more negative adsorption energy. Charge density difference due to O_2 adsorption was obtained as

$$\Delta\rho = \rho - \rho(\mathrm{Au}_N/\mathrm{TiO}_2) - \rho(\mathrm{O}_2) \qquad (1)$$

where ρ is the charge density of the whole system, and $\rho(Au_N/TiO_2)$ and $\rho(O_2)$ are those of Au_N/TiO_2 and a

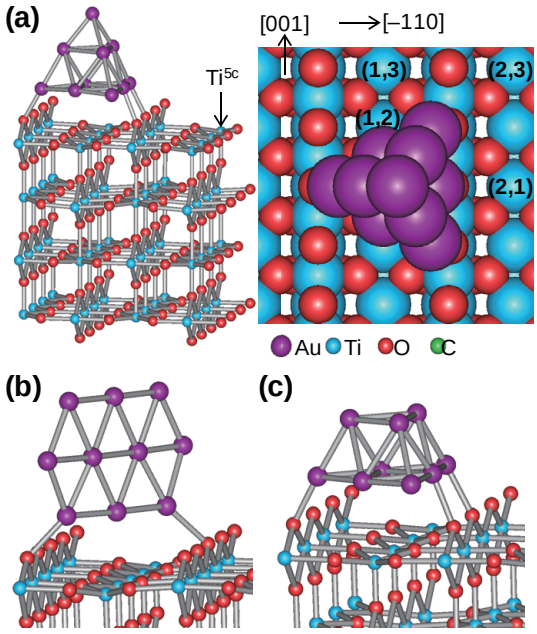

FIG. 1. Models for a TiO_2(110)-supported Au cluster. (a) Tetrahedral Au_{10}. Indices for Ti^{5c} sites are displayed in a plan view (right). (b) Planar Au_{10}. (c) Truncated pyramidal Au_9 (doublet).

spin-polarized O_2, respectively, calculated using the same cell and atomic coordinates as in the whole system.

The accuracy of the present calculation has been estimated as follows. The uncertainty associated with the cell size would be ∼ 0.06 eV because difference in O_2 adsorption energies between $Ti^{(2,3)}$ and $Ti^{(2,1)}$ is 0.12, 0.16, and 0.06 eV for 2×4, 2×5, and 3×4 cells, respectively (all sampled at 1×2 k-point mesh). Dependence on the slab thickness and k-point mesh would be similar to that (∼ 0.03 eV) found for the supported rod [18].

III. Au_{10}/TiO_2 MODEL

A. O_2 adsorption

Earlier DFT studies [9,10,17,18] on TiO_2-supported Au clusters and nanorods have found that O_2 adsorbs strongly to the Ti^{5c} site in a sideon configuration (Ti–O_2). This is also the case for Au_{10}: O_2 adsorbs sideon to the $Ti^{(2,1)}$ site with a very strong adsorption energy of -2.35 eV (Fig. 2(a)). Strong O_2 activation can be seen in a substantial increase in the O-O bond length and negative charge carried by O_2. The upward displacement of Ti^{5c} (by 95 pm) and the orientation of the O-O bond (47° with respect to TiO_2[001]) indicate strong orbital interactions between O_2 and Ti^{5c}. To analyze this further, we have calculated projected density of states (PDOS) for the Ti atom and the O of O_2 (Fig. 3(a)). An overlap between O p_z and Ti d_{xz} states around -1.4 eV indicates a π-type interaction between the out-of-plane O_2 π^* and Ti 3d orbitals. An overlap between O p_y and Ti d_{xy} states around -0.2 eV indicates a δ-type interaction between the in-plane O_2 π^* and Ti 3d orbitals; the diagonal orien-

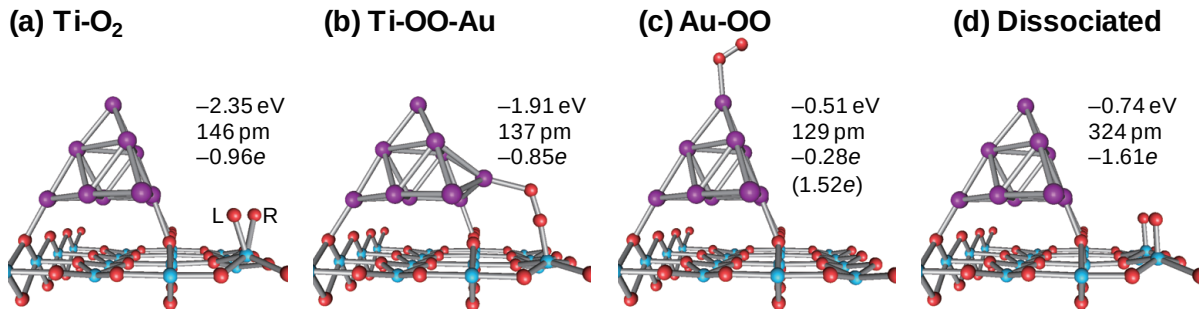

FIG. 2. O_2 adsorption configurations. (a) O_2 sideon to $Ti^{(2,1)}$. (b) O_2 between $Ti^{(2,1)}$ and Au sites. (c) O_2 on the apex. (d) O_2 dissociation between Ti sites. Adsorption energies, O–O lengths, and Bader charges (spin charges) on O_2 are displayed in the figure.

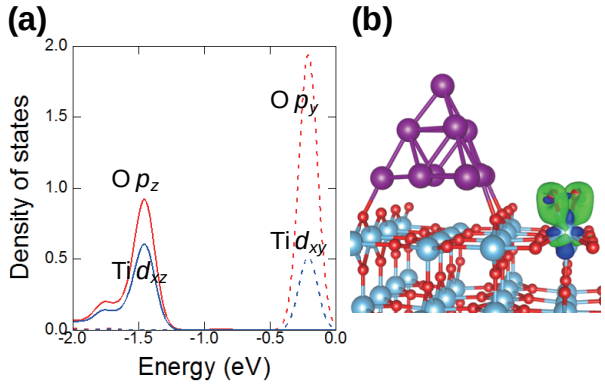

FIG. 3. Electronic state of $Ti^{(2,1)}$–O_2. (a) Density of states projected onto $Ti^{(2,1)}$ and the left O of O_2. Left and right O are actually indistinguishable in PDOS. The Fermi level is at 0 eV. The xy axis is rotated 45° around [110] from [$\bar{1}$10] and [001] directions. (b) Charge density difference due to O_2 adsorption. Green and blue surfaces are isosurfaces drawn at $+0.01e$/Bohr^3 and $-0.01e$/Bohr^3, respectively.

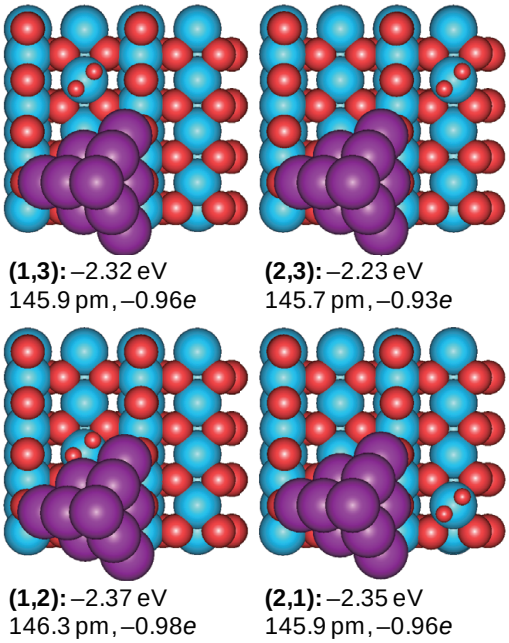

FIG. 4. Sideon O_2 on various Ti^{5c} sites (plan view). Adsorption energies, O–O lengths, and Bader charges on O_2 are displayed in the figure.

tation of O-O is key to this interaction. With both π^* orbitals lowered below the Fermi level, O_2 is activated to a peroxide state. This can also be seen in the charge density difference due to O_2 adsorption (Fig. 3(b)): As a result of electron transfer to both π^* orbitals, a ring-shaped region of electron accumulation appears on each O of O_2. A spin-polarized calculation also confirms that O_2 is in a singlet state. We add that, in spite of the O-O bond weakening, O_2 dissociation between two Ti sites is unlikely because the resulting configuration is much less stable (Fig. 2(d)).

O_2 adsorbs at a dual perimeter site consisting of $Ti^{(2,1)}$ and Au sites (Ti–OO–Au) with a strong adsorption energy of -1.91 eV (Fig. 2(b)). O_2 activation is not so strong as in Ti–O_2. The striking feature of this configuration is that O_2 extrudes a Au atom out of the cluster, causing the cluster to shrink by 10% along the TiO_2[001] direction. Extrusion by O_2 is barely noticeable on the Au rod [18] because a continuous structure would be unable to accommodate the resulting strain. Compared to the one on the rod model, the present Ti–OO–Au has a shorter Au-O_2 distance (214 vs. 240 pm) and a more relaxed Ti–O–O bond angle (173° vs. 162°). As a result, the energy difference between Ti–O_2 and Ti–OO–Au decreases from 0.71 eV [18] to 0.44 eV, although Ti–O_2 is still the more stable configuration.

Compared to these Ti-adsorbed ones, O_2 on the apex of Au_{10} is much less stable, with an adsorption energy of -0.51 eV (Fig. 2(c)). This O_2 is barely activated, as can be seen in the O-O bond length and the charge and spin it carries. In addition, the positive charge induced on the top Au atom is small ($+0.13e$), indicating the weakness of the Au-O_2 ionic bonding.

Having confirmed the greater stability of the sideon configuration, we now examine the relative stability between various Ti^{5c} sites (Fig. 4). $Ti^{(1,2)}$–O_2 is practically degenerate with $Ti^{(2,1)}$–O_2 in spite of a contact with the Au cluster. $Ti^{(1,3)}$–O_2 is not directly next to the cluster, but is only marginally less stable than the on-perimeter ones. $Ti^{(2,3)}$–O_2 is slightly less stable than $Ti^{(2,1)}$–O_2. The O-O bond length and negative charge on O_2 are sim-

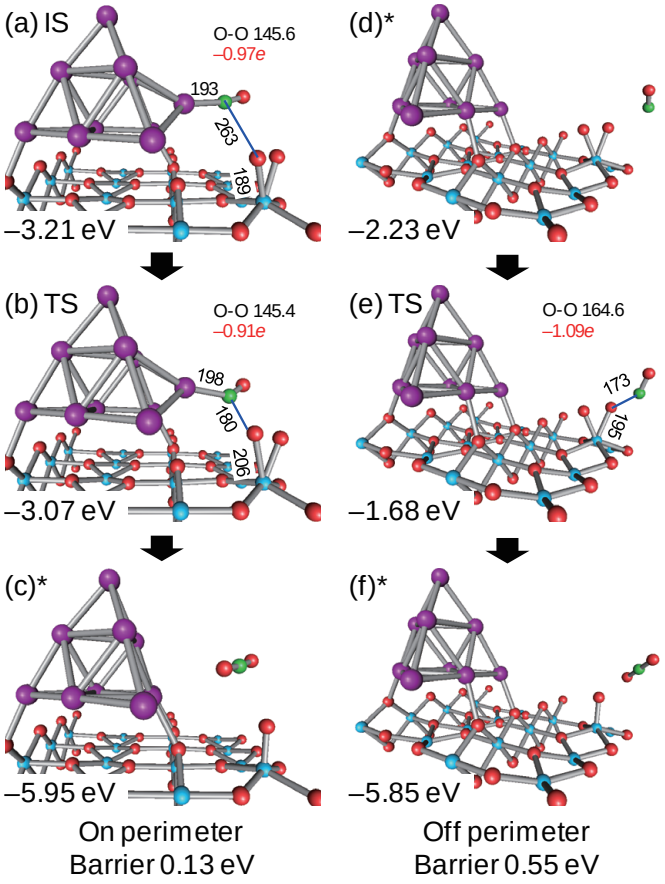

FIG. 5. O_2 + CO reaction on and off the perimeter. (a-c) $Ti^{(2,1)}$–O_2 reacting with Au–CO. (d-f) $Ti^{(2,3)}$–O_2 reacting with CO(g). Adsorption energies, interatomic distances (pm), and Bader charges on O_2 and O adatoms are displayed in the figure. For a desorption state (marked with $*$), a snapshot is presented along with the energy at the desorption limit.

ilar for all the Ti–O_2. The stability and activation state of Ti–O_2 thus depends weakly on distance to the Au cluster.

B. CO oxidation

As a typical example of CO oxidation on the perimeter of a Au cluster, we have examined a process whereby $Ti^{(2,1)}$–O_2 reacts with CO adsorbed on the adjacent Au site (Figs. 5(a), (b), and (c)). As the figures show, CO approaches the left O of O_2 on its C end, extract the O to form CO_2, which desorbs spontaneously. The O adatom left on the Ti site is expected to react readily with CO [13]. Compared to the rod model [18], the calculated energy barrier for the Ti–O_2 + Au–CO step is smaller (0.13 vs. 0.22 eV). It is difficult to explain such a small difference, although a possible cause seems to be the extrusion of a Au atom by CO (Fig. 5(a)); extrusion by CO is noted in earlier work on free Au clusters [29]. In the Au_{10} model, the Au atom is already extruded at IS, so it needs not be extruded further in going to TS. In the rod model, the corresponding Au atom must be extruded by 11 pm in going from IS to TS.

As an example of CO oxidation over an off-perimeter site, we have examined a direct reaction between $Ti^{(2,3)}$–O_2 and CO(g) (Figs. 5(d), (e), and (f)). The calculated energy barrier of this reaction, 0.55 eV, is very close to 0.56 and 0.57 eV we obtained for Ti–O_2 + CO(g) reaction at the first and second nearest Ti site of the supported rod model, respectively [18]. Without CO activation by the Au [18], the reaction depends heavily on O_2 activation, as can be seen in O-O stretching and negative charge on O_2 at TS (Fig. 5(e)). Because the state of O_2 activation differs little between various Ti^{5c} sites (Fig. 4) and Au models, a similar barrier can be expected for Ti–O_2 + CO(g) reactions.

IV. Au_9/TiO_2 MODEL

For comparison, we have also examined CO oxidation over the Au_9 model. Results for $Ti^{(2,1)}$–O_2 + Au–CO reaction are presented in Fig. 6(a). As is the case with Au_{10}, CO extracts the left O of O_2 to form CO_2. IS and TS are similar to those found for Au_{10}. In particular, O_2 is activated to a similar extent despite the odd number of electrons in the system; such a trend is also reported for Au_9 and Au_{10} strips [17]. As a result, the energy barrier (0.11 eV) is very close to that for Au_{10}. Furthermore, the calculated barrier for $Ti^{(2,3)}$–O_2 + CO(g) reaction is again 0.55 eV. Thus, O_2 + CO reaction is faster at the perimeter also for Au_9.

However, CO_2 formed by the $Ti^{(2,1)}$–O_2 + Au–CO reaction interacts differently with the cluster, combining with the remaining O adatom to form a carbonate, which is bound to two Au sites and the $Ti^{(2,1)}$ site (FS of Fig. 6(a)). Bader analysis indicates that an O adatom on $Ti^{(2,1)}$ receives the same amount of negative charge ($-0.89e$) whether the cluster is Au_9 or Au_{10}. On the other hand, the Au_9 cluster is in a spin-polarized state (Fig. 6(c)), with a spin charge of $0.87e$, and so CO_2 does not detach from Au_9 as readily as it does from Au_{10}. This leaves some room for CO_2 to react with the O adatom. The implication is that a carbonate may form on odd-numbered clusters, although more calculations are needed for confirmation.

The decomposition of the carbonate into CO_2(g) and an O adatom is unfavorable by 0.39 eV. Thus, the carbonate may inhibit CO oxidation by rendering unavailable active Ti sites. Water may assist its decomposition [30] or prevent it from forming. Indeed, our calculations (Fig. 6(b)) indicate that, if H_2O is adsorbed on a Ti site next to O_2, the barrier of the $Ti^{(2,1)}$–O_2 + Au–CO reaction does not change much (0.16 eV), but CO_2 desorbs instead of forming a carbonate. Apparently, hydrogen bonding with H_2O renders the O adatom less reactive with CO_2.

V. CONCLUSIONS

In this plane-wave DFT study, we have examined CO oxidation on a rutile TiO_2(110) surface supporting sub-nanometer Au clusters. We mainly studied tetrahedral Au_{10} and also a truncated pyramidal Au_9. We have found that O_2 adsorbs sideon to a pentacoordinate Ti site (Ti–O_2), activated to a peroxide state. This O_2 is more stable than O_2 at a Ti–Au dual-perimeter site or O_2 on the apex of the cluster. Moreover, the stability of sideon O_2

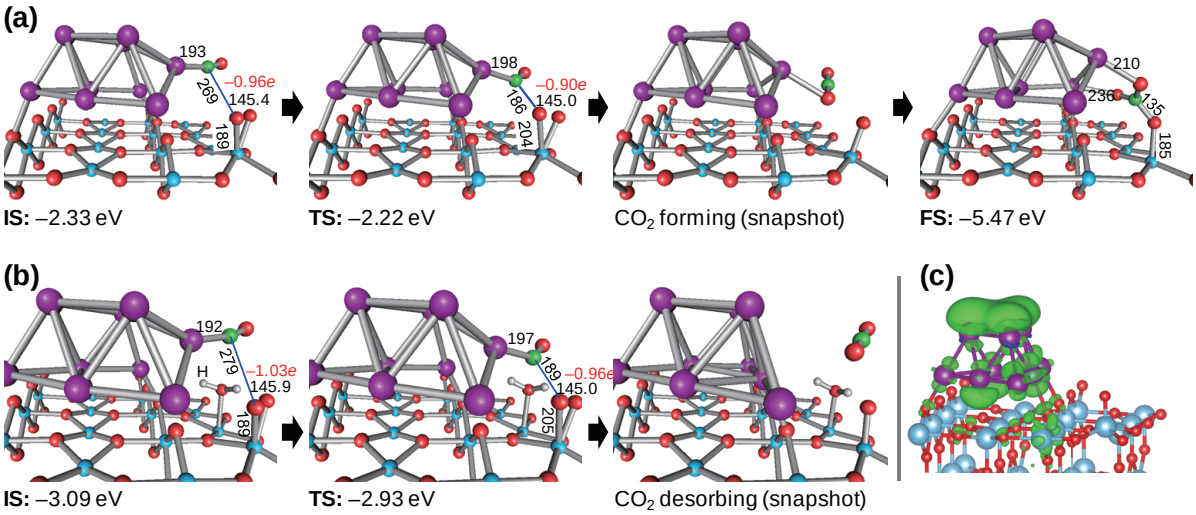

FIG. 6. $Ti^{(2,1)}$–O_2 + Au–CO reaction over Au_9/TiO_2. Adsorption energies, interatomic distances (pm), and Bader charges on O_2 are displayed in the figure. (b) Same with H_2O adsorbed next to O_2. (c) Spin charge density plot for Au_9/TiO_2 with an O adatom on $Ti^{(2,1)}$. Green and blue surfaces are isosurfaces drawn at $+0.001e$/Bohr^3 and $-0.001e$/Bohr^3, respectively.

depends weakly on distance to the Au cluster. Thus, O_2 adsorption is dominated by the interaction with Ti sites, although the Au cluster is still essential as an electron donor to O_2. The trend is similar to what we have found for the supported Au nanorod [18].

For Ti–O_2 + Au–CO reaction, similar barriers have been found for Au_9 and Au_{10} (0.11 and 0.13 eV, respectively). These barriers are slightly lower than 0.22 eV found for the rod [18]. After the reaction, CO_2 desorbs from Au_{10} while a carbonate forms on Au_9. We have also found that more remote Ti–O_2 reacts with CO(g) with a barrier of 0.55 eV on both Au_9 and Au_{10}. The barrier of this size appears to be universal for various Ti–O_2 and Au models.

In conclusion, O_2 + CO reaction is much faster at the perimeter even for small FCC clusters such as Au_9 and Au_{10}. However, the interaction of product CO_2 with the surface is more dependent on the size and shape of the cluster, sometimes yielding a carbonate.

ACKNOWLEDGMENTS

This work was performed under a management of 'Elements Strategy Initiative for Catalysts and Batteries (ESICB)' supported by Ministry of Education, Culture, Sports, Science, and Technology, Japan (MEXT).

[1] M. Haruta, N. Yamada, T. Kobayashi, and S. Iijima, J. Catal. **115**, 301 (1989).
[2] M. Okumura, S. Nakamura, S. Tsubota, T. Nakamura, M. Azuma, and M. Haruta, Catal. Lett. **51**, 53 (1998).
[3] T. Takei, T. Akita, I. Nakamura, T. Fujitani, M. Okumura, K. Okazaki, J. H. Huang, T. Ishida, and M. Haruta, Adv. Catal. **55**, 1 (2012).
[4] M. Haruta, Catal. Today **36**, 153 (1997).
[5] M. Kotobuki, R. Leppelt, D. A. Hansgen, D. Widmann, and R. J. Behm, J. Catal. **264**, 67 (2009).
[6] T. Fujitani and I. Nakamura, Angew. Chem. Int. Ed. **50**, 10144 (2011).
[7] P. Hohenberg and W. Kohn, Phys. Rev. B **136**, B864 (1964).
[8] W. Kohn and L. J. Sham, Phys. Rev. **140**, 1133 (1965).
[9] Z.-P. Liu, X.-Q. Gong, J. Kohanoff, C. Sanchez, and P. Hu, Phys. Rev. Lett. **91**, 266102 (2003).
[10] L. M. Molina, M. D. Rasmussen, and B. Hammer, J. Chem. Phys. **120**, 7673 (2004).
[11] I. N. Remediakis, N. Lopez, and J. K. Norskov, Angew. Chem. Int. Ed. **44**, 1824 (2005).
[12] J. Wang and B. Hammer, Phys. Rev. Lett. **97**, 136107 (2006).
[13] I. X. Green, W. Tang, M. Neurock, and J. T. Yates, Jr., Science **333**, 736 (2011).
[14] Y.-G. Wang, Y. Yoon, V.-A. Glezakou, J. Li, and R. Rousseau, J. Am. Chem. Soc. **135**, 10673 (2013).
[15] L. Li, Y. Gao, H. Li, Y. Zhao, Y. Pei, Z. F. Chen, and X. C. Zeng, J. Am. Chem. Soc. **135**, 19336 (2013).
[16] L. Li and X. C. Zeng, J. Am. Chem. Soc. **136**, 15857 (2014).
[17] S. Chrétien and H. Metiu, J. Chem. Phys. **128**, 044714 (2008).
[18] H. Koga, K. Tada, and M. Okumura, Chem. Phys. Lett. **610-611**, 76 (2014).
[19] Y. Morikawa, H. Ishii, and K. Seki, Phys. Rev. B **69**, 041403 (2004).
[20] K. Okazaki, Y. Morikawa, S. Tanaka, K. Tanaka, and M. Kohyama, Phys. Rev. B **69**, 235404 (2004).
[21] K. Tada, K. Sakata, S. Yamada, K. Okazaki, Y. Kitagawa, T. Kawakami, S. Yamanaka, and M. Okumura, Mol. Phys. **112**, 365 (2014).
[22] D. Vanderbilt, Phys. Rev. B **41**, 7892 (1990).
[23] J. P. Perdew, K. Burke, and M. Ernzerhof, Phys. Rev. Lett. **77**, 3865 (1996).
[24] Y. Tateyama, T. Ogitsu, K. Kusakabe, and S. Tsuneyuki, Phys. Rev. B **54**, 14994 (1996).
[25] R. Bader, Atoms in Molecules: A Quantum Theory (Ox-

ford University Press, New York, 1990).
[26] G. Henkelman, A. Arnaldsson, and H. Jonsson, Comput. Mater. Sci. **36**, 354 (2006).
[27] K. Momma and F. Izumi, J. Appl. Crystallogr. **44**, 1272 (2011).
[28] T. Akita, K. Tanaka, M. Kohyama, and M. Haruta, Surf. Interface Anal. **40**, 1760 (2008).
[29] H. J. Zhai, L. L. Pan, B. Dai, B. Kiran, J. Li, and L. S. Wang, J. Phys. Chem. C **112**, 11920 (2008).
[30] M. Date, M. Okumura, S. Tsubota, and M. Haruta, Angew. Chem. Int. Ed. **43**, 2129 (2004).